Negative Refraction, Growing Evanescent Waves, and Sub-Diffraction Imaging in Loaded Transmission-Line Metamaterials

Anthony Grbic, *Student Member, IEEE,* and George V. Eleftheriades, *Senior Member, IEEE*

***Abstract*—We present an analytical formulation that shows the negative refraction of propagating waves and the growth of evanescent waves within a negative refractive index (NRI) lens made of a periodically L, C loaded transmission-line (TL) network, referred to as the dual-TL structure. A transformation known as the "array scanning method" is then employed to analytically demonstrate the sub-diffraction imaging capability of a dual-TL lens. In essence, the two-dimensional (2-D) periodic Green's functions corresponding to the voltages and currents excited by a vertical elementary current source are derived. The developed theory is utilized to plot the 2-D voltage magnitude distribution for the case of focusing an elementary current source. The analysis reveals that a resolution limit is imposed by the periodicity of the NRI medium used. Moreover, the periodicity of the NRI medium bounds the amplitude of the growing evanescent waves in a realizable NRI lens and prevents them from growing to unphysically large values.**

***Index Terms*—Left-handed media, metamaterials, negative refractive index (NRI), periodic structures, printed circuits, sub-diffraction imaging, transmission lines (TLs).**

I. INTRODUCTION

IN THE 1960s, Veselago theoretically investigated the electrodynamics of substances possessing negative permittivity (ϵ) and permeability (μ) [1]. Among other things, Veselago showed that a planar slab of material with $\epsilon < 0, \mu < 0$ possesses a negative refractive index (NRI) and acts as an unusual lens that focuses rays of light emanating from a source to an image on the opposite side of the slab. Pendry's more recent prediction that such slabs act as "perfect lenses" rekindled interest in materials with negative material parameters (ϵ, μ) [2]. Pendry revealed that the flat lens described by Veselago focuses all the Fourier components emanating from a source including the evanescent waves. As a result, these "perfect lenses" achieve sub-diffraction focusing. Pendry's analysis was stimulated by the implementation of an NRI metamaterial [3]. The initial NRI metamaterial employed metallic wires to achieve negative permittivity and split-ring resonators to achieve negative permeability. It was used to demonstrate a "left handed" (backward-wave propagation) band and to experimentally verify negative refraction.

The authors are with The Edward S. Rogers Sr. Department of Electrical and Computer Engineering, University of Toronto, Toronto, ON, Canada M5S 3G4 (e-mail: grbica@waves.utoronto.ca; gelefth@waves.utoronto.ca).
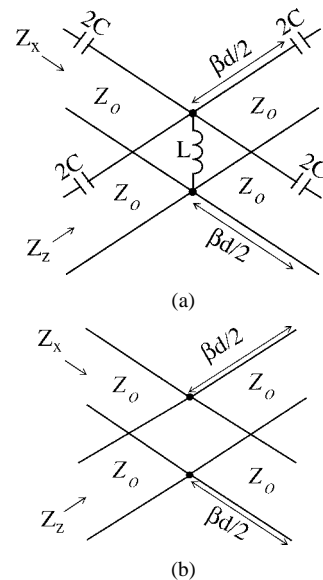
Fig. 1.   TL unit cells.

Last year, the periodic two-dimensional (2-D) L, C loaded transmission-line (TL) network depicted in Fig. 1(a) was also shown to act as an isotropic "left handed" or NRI medium [4]–[6]. This distributed network was termed a dual TL due to its high-pass configuration, as opposed to the low-pass representation of a conventional TL. One-dimensional dual TLs that have been known for some time [7] were revived in [8]–[10] and directly related to NRI materials. Focusing within a 2-D microstrip-based dual-TL structure was experimentally demonstrated at microwave frequencies and a coplanar waveguide (CPW) implementation was also used to experimentally verify leaky backward-wave radiation from its fundamental spatial harmonic [5], [11], [12]. Additionally, simulation results have been reported showing negative refraction at the interface of a TL mesh medium [shown in Fig. 1(b)] acting as the positive refractive index (PRI) medium, and a dual-TL structure [4], [13]. Growing evanescent waves within a dual-TL structure have been recently demonstrated in [14]. A Bloch formulation has also been developed in [13] to determine the 2-D dispersion characteristics of the dual-TL structure.

Alternatively, anisotropic structures that achieve sub-wavelength focusing have been experimentally investigated in [15] and similar concepts theoretically shown in [16]. In these structures, however, the source and focus are embedded in complementary anisotropic metamaterials, therefore, this type of focusing cannot be extended to free space.
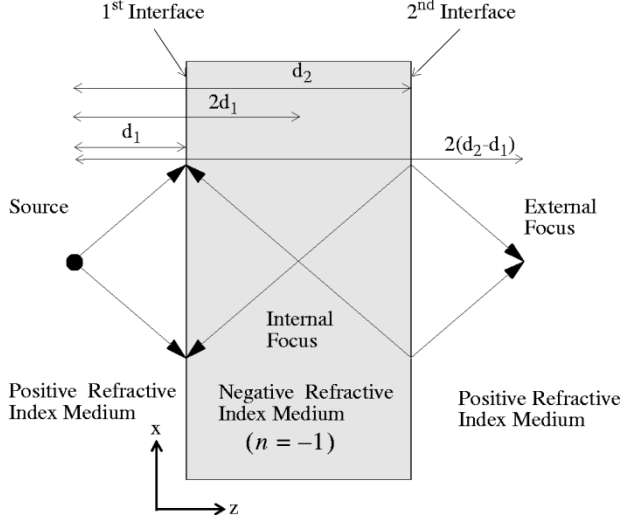
Fig. 2. Veselago's flat lens.

In this paper, we present an exact analytical formulation that confirms the negative refraction of propagating (homogeneous) waves and the growth of evanescent (inhomogeneous) waves within a planar isotropic NRI lens made of a dual-TL structure. These results are then combined with the "array scanning method" of [17], [18] to analytically show sub-diffraction imaging by a dual-TL lens from one isotropic medium to another. To show sub-diffraction imaging, the 2-D periodic Green's functions corresponding to the voltages and currents excited by a vertical elementary current source in the entire TL structure is derived. The analysis predicts that a resolution limit is imposed by the periodicity of the NRI and PRI media used. This resolution limit is not revealed by the analysis of continuous NRI lenses in [11] and [19]–[21]. The developed theory is utilized to plot the 2-D voltage magnitude distribution for the case of focusing an elementary current source. These plots reveal that the three-region lens examined in this paper is quite distinct from the experimental lenses reported in [5], [22], which utilized a single interface between an NRI medium and a PRI medium (two-region lenses). The two-region lens arrangement did not permit the proper growth of evanescent waves necessary to clearly achieve sub-diffraction imaging. Finally, it is shown that the periodicity of the NRI medium bounds the amplitude of the growing evanescent waves in a practical NRI lens of finite thickness and prevents them from growing to unphysically large values.

II. "PERFECT" LENS AND ITS TL IMPLEMENTATION

Veselago's flat lens made of a slab of NRI material is shown in Fig. 2. The imaging of a monochromatic source within a PRI medium is depicted. The rays indicate the negative refraction of the propagating waves as described by Veselago. They suggest that two foci exist. There is an internal focus ($z = 2d_1$) within the lens and an external focus ($z = 2d_2 - 2d_1$) beyond the second interface of the lens. In addition to focusing the propagating Fourier components, Pendry pointed out that the evanescent Fourier components decaying from the source are

also restored at the external focal plane. The evanescent components grow within the NRI lens, thus canceling the decay experienced in the positive refractive media on either side of the lens. Due to these growing evanescent waves, the field amplitudes are highest at the second interface of the lens [14]. The "perfect focusing" predicted by Pendry, however, only occurs when certain criteria are met. The lens must be lossless and its relative refractive index must be -1 with respect to the two surrounding PRI half-spaces to eliminate aberrations, and the lens must be impedance matched to each half-space to eliminate reflections.

Both the PRI and NRI media considered in this paper are TL-based periodic structures. The PRI medium is the 2-D network of TLs shown in Fig. 1(b), which will be referred to as a TL mesh. The NRI medium is the dual-TL structure depicted in Fig. 1(a). Both the TL mesh and dual-TL structure are operated at frequencies of homogeneous and isotropic propagation and, therefore, can be justifiably called effective media. At these frequencies, the dual-TL structure exhibits backward-wave propagation characteristics and the TL mesh forward-wave propagation characteristics, as would an NRI and PRI medium, respectively [13]. The propagation characteristics of the two media are best described by their respective dispersion relations and Bloch impedance expressions, which have been derived in [13]. The dispersion relation for the TL mesh is given by the following expression [13]:

$$\sin^2\left(\frac{k_x d}{2}\right) + \sin^2\left(\frac{k_z d}{2}\right) = 2\sin^2\left(\frac{\beta d}{2}\right) \qquad (1)$$

where k_x and k_z are the wavenumbers in the x- and z-directions, respectively, d is the unit cell dimension, and β is the propagation constant of the interconnecting TL sections. The wavenumber k_x and k_z are simply the x and z components of the intrinsic wavenumber k_p of the medium

$$k_x = k_p \sin(\phi) \quad k_z = k_p \cos(\phi) \qquad (2)$$

where ϕ is angle between $\vec{k}_p$ and the z-axis. The Bloch impedances in the x- and z-directions for the TL mesh are [13]

$$Z_{xp} = Z_o \frac{\tan\left(\frac{\beta d}{2}\right)}{\tan\left(\frac{k_x d}{2}\right)} \quad Z_{zp} = Z_o \frac{\tan\left(\frac{\beta d}{2}\right)}{\tan\left(\frac{k_z d}{2}\right)} \qquad (3)$$

where ω is the radial frequency and Z_o is the characteristic impedance of the interconnecting TL sections. The dispersion relation for the dual-TL structure shown in Fig. 1(a) can also be derived using Bloch analysis [13]. It is given by the following expression:

$$\sin^2\left(\frac{k_x d}{2}\right) + \sin^2\left(\frac{k_z d}{2}\right)$$
$$= \frac{1}{2}\left[2\sin\left(\frac{\beta d}{2}\right) - \frac{1}{Z_o \omega C}\cos\left(\frac{\beta d}{2}\right)\right]$$
$$\times \left[2\sin\left(\frac{\beta d}{2}\right) - \frac{Z_o}{2\omega L}\cos\left(\frac{\beta d}{2}\right)\right] \qquad (4)$$

where L is the shunt loading inductance and C is the series loading capacitance of the dual-TL structure, shown in Fig. 1(a).

$k_p d = -k_n d$	$Z_{xp}(k_z = 0) = Z_{xn}(k_z = 0)$	Z_o	βd	L	C
$0.3491\,rad$	$50.000\,\Omega$	$71.25730\,\Omega$	$0.246200\,rad$	$11.45777\,nH$	$4.513061\,pF$

The wavenumbers k_x and k_z once again can be expressed in terms of the intrinsic wavenumber of the medium k_n

$$k_z = k_n \cos(\phi) \quad k_x = k_n \sin(\phi) \tag{5}$$

where ϕ is angle between $\vec{k}_n$ and the z-axis. The Bloch impedances in the x- and z-directions for the dual-TL structure are given by the following expressions:

$$Z_{xn} = \frac{Z_o \tan\left(\dfrac{\beta d}{2}\right) - \dfrac{1}{2\omega C}}{\tan\left(\dfrac{k_x d}{2}\right)}$$

$$Z_{zn} = \frac{Z_o \tan\left(\dfrac{\beta d}{2}\right) - \dfrac{1}{2\omega C}}{\tan\left(\dfrac{k_z d}{2}\right)}. \tag{6}$$

In order to implement Pendry's perfect lens using the TL mesh and dual-TL structure, a few requirements must be met. Both structures must behave as effective media with homogeneous and nearly isotropic propagation characteristics. It is clear from the dispersion relations (1) and (4) that such propagation characteristics exist when $k_x d \ll 1$, $k_z d \ll 1$, and $\beta d \ll 1$. Another requirement is that the relative refractive index between the TL mesh and dual-TL structure must be -1. This can be achieved by making the intrinsic wave vectors $\vec{k}_p$ in the TL mesh and $\vec{k}_n$ in the dual-TL structure equal in magnitude, but antiparallel for all directions of power flow. Lastly, the Bloch impedances of the TL mesh and the dual-TL structure must be equal for all angles of incidence in order to eliminate reflections. Table I lists the electrical parameters of a TL mesh and dual-TL structure that exhibit homogeneous and nearly isotropic propagation characteristics. They are impedance matched and have a relative refractive index of -1 with respect to each other at a frequency of 1 GHz. For simplicity, the same TL parameters (Z_o and βd) are utilized in both structures. The TL mesh and dual-TL structure differ only in terms of the shunt L and series C loading parameters.

Fig. 3 shows the magnitude of the wavenumbers (k_p and k_n) for all directions of propagation at 1 GHz in the TL mesh and dual-TL structure defined in Table I. It is evident from the plot that the magnitude of the refractive index is the same for both structures since the two curves overlap. The structures are nearly isotropic since the plots appear circular, indicating that the magnitudes of $\vec{k}_p$ and $\vec{k}_n$ change very little with the direction of propagation ϕ. In fact, the maximum change in wavenumber with respect to ϕ for both structures is 0.26%. It is also important to note that, for any direction of power flow, the wave vectors in the two media are antiparallel. The z-directed Bloch impedances (Z_{zp}, Z_{zn}) have been plotted in Fig. 4(a) as a function of propagation direction ϕ. Due to the symmetry of the unit cells,
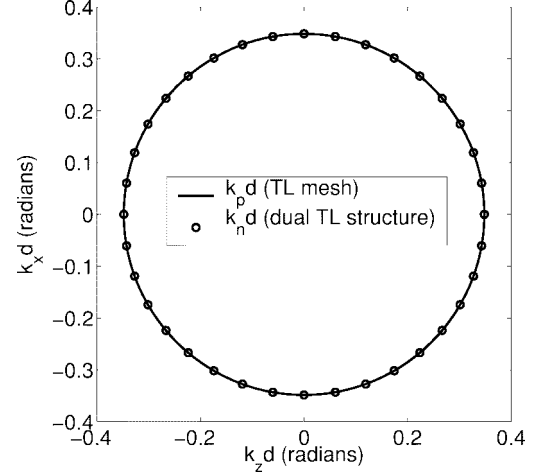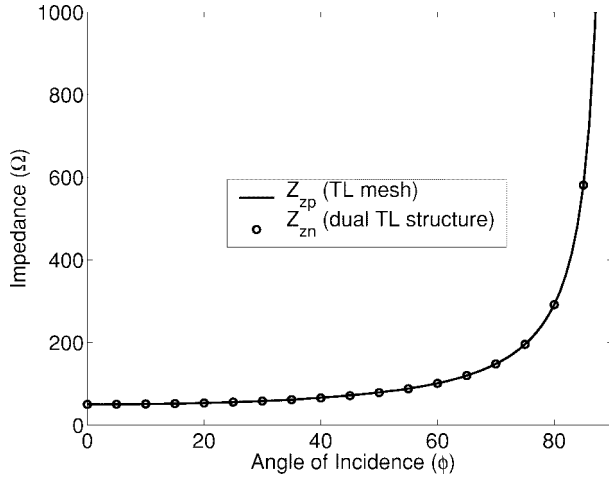

Fig. 3. Wavenumber as a function of incident angle.

the Bloch impedances are plotted only for $\phi = 0°$ to $90°$. The impedances asymptotically approach infinity at $90°$ since the z-directed current is zero for a plane wave propagating along the x-axis. The x-directed Bloch impedances (Z_{xp}, Z_{xn}) for both media are shown in Fig. 4(b). In this case, the impedance asymptotically approaches infinity for $\phi = 0$ since the x-directed current is zero for plane-wave propagation along the z-axis. Most importantly, Figs. 4(a) and (b) show that in addition to having refractive indexes that are equal and opposite, the two media are matched for all angles of propagation. In effect, we have shown that the TL mesh and dual-TL structure are suitable PRI and NRI media for realizing Pendry's "perfect lens." The flat lens system depicted in Fig. 2 could, therefore, be implemented using these two periodic structures.

III. PLANE-WAVE REFLECTION AND REFRACTION

In this section, plane-wave incidence on an NRI lens is investigated specifically for TL metamaterials. The NRI lens of Fig. 2 is a 2-D dual-TL structure and the surrounding PRI medium is a TL mesh, as shown in Fig. 5. The incident plane wave is a voltage/current wave incident from the TL mesh. A plane-wave excitation is achieved using an infinite array of current sources, as shown in Fig. 5. Voltage solutions are derived for the distributed network shown in Fig. 5 for different plane-wave excitations to demonstrate negative refraction and the growth of evanescent waves. In addition, these results are utilized in the following section to derive the Green's functions of the lens system in Fig. 5: the voltage and current solutions due to a single current source.

The dual-TL lens depicted in Fig. 5 is finite in the z-direction and infinite in the x-direction. The PRI media on either side of the lens are semi-infinite TL meshes. For clarity, the 2-D space is divided into four regions. Region A extends from $-\infty \le z \le 0$
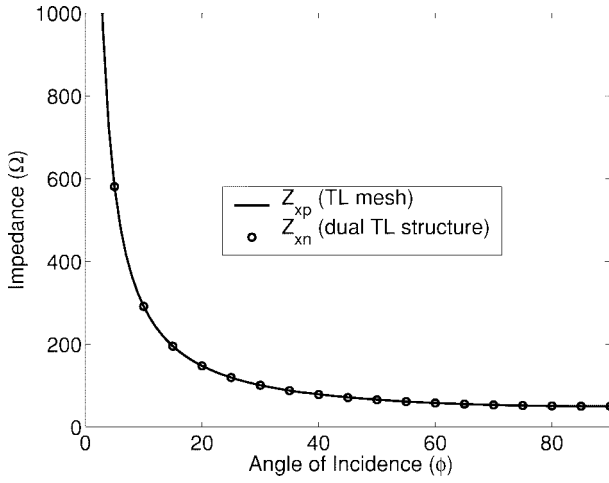
Fig. 4.   Bloch impedance as a function of incident angle (ϕ).

Fig. 5.   Veselago's flat lens system using TL metamaterials.

and region B extends from $0 \leq z \leq hd$, where h is a positive integer. Regions A and B are composed of the same TL mesh. For both regions, the x- and z-directed Bloch impedances will be referred to as Z_{xa} and Z_{za}, respectively. The wave vector will be labeled $\vec{k}_a$ and the x- and z-directed wavenumbers k_{xa} and k_{za}, respectively. Region C encompasses the NRI lens made of the dual-TL structure. It extends from $hd \leq z \leq ld$, where l is also a positive integer. Similarly, the Bloch impedances for this region are labeled Z_{xc} and Z_{zc}, the wave vector $\vec{k}_c$, and the wavenumbers k_{xc} and k_{zc}. The TL mesh on the opposite side of the lens ($ld \leq z \leq \infty$) will be referred to as region D. Following the same convention, the Bloch impedances for region D are Z_{xd} and Z_{zd}, the wave vector $\vec{k}_d$, and the wavenumbers k_{xd} and k_{zd}. The Bloch impedances in regions A, B, and D are given by the Bloch impedance expressions for a TL mesh (3) and the Bloch impedances in region C are given by the Bloch impedance expressions for a dual-TL structure (6). Similarly, the wavenumbers in regions A, B, and D are given by (1) and those in region C are given by (4).

An infinite array of y-directed current sources is placed along the x-axis to provide a plane-wave excitation. The current sources have equal amplitude I_o and possess a progressive phase shift of $-\xi$. In general, a current source at coordinate $(x, z) = (rd, 0)$ has a corresponding phase shift of $-r\xi$, where
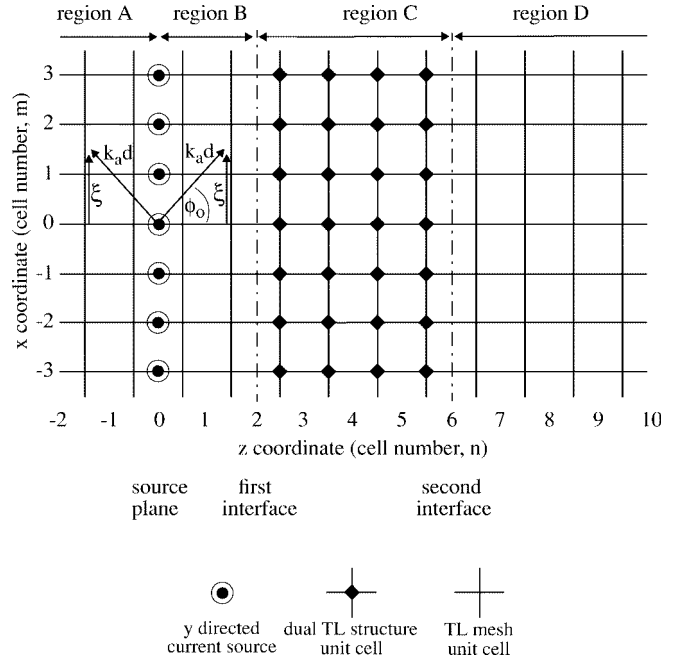
r is an integer. The infinite array of current sources in fact excites two plane waves in the homogeneous, nearly isotropic TL mesh. One plane wave in region A and one plane wave in region B, both propagating away from the current source array. The plane wave in region B has a propagation direction ϕ_o given by the following expression familiar from antenna array analysis:

$$\phi_o = \sin^{-1}\left(\frac{\xi}{k_a d}\right). \tag{7}$$

The direction of propagation for the plane wave excited in region A is $\pi - \phi_o$. The boundary between regions B and C will be referred to as the first interface. The first interface is located at a distance $z = hd$ ($h = 2$ in Fig. 5), which corresponds to the distance $z = d_1$ in Fig. 2. Likewise, the boundary between regions C and D will be referred to as the second interface. It is located at a distance $z = ld$ ($l = 6$ in Fig. 5) and corresponds to $z = d_2$ in Fig. 2. The progressive phase shift between the current sources dictates that $k_{xa}d = k_{xc}d = k_{xd}d = \xi$ in the four regions of interest. Given the current array excitation, the voltage at a point $(x, z) = (md, nd)$ (where m and n are integer values) can be represented as a sum of an incident and reflected voltage plane waves within each region. The voltage solution takes on the following form if a time harmonic variation of the form $e^{j\omega t}$ is assumed:

$$V(md, nd) = V_1 e^{jk_{za}nd} e^{-jm\xi}, \qquad z \leq 0 \text{ (region A)}$$

$$V(md, nd) = \left[V_2 e^{-jk_{za}nd} + V_3 e^{jk_{za}nd}\right] e^{-jm\xi},$$
$$0 \leq z \leq hd \text{ (region B)}$$

$$V(md, nd) = \left[V_4 e^{-jk_{zc}(n-h)d} + V_5 e^{jk_{zc}(n-h)d}\right] e^{-jm\xi},$$
$$hd \leq z \leq ld \text{ (region C)}$$

$$V(md, nd) = V_6 e^{-jk_{zd}(n-l)d} e^{-jm\xi},$$
$$z \geq ld \text{ (region D)}. \tag{8}$$

The voltage coefficients of the incident waves (V_2, V_4, V_6) and those of the reflected waves V_1, V_3, V_5 are given by the following expressions:

$$
\begin{aligned}
V_1 &= V_2 + V_3 \\
V_2 &= \frac{I_o Z_{za}}{2} \\
V_3 &= \frac{V_2 e^{-2jk_{za}hd}\left[\Gamma_1 + \Gamma_2 e^{-2jk_{zc}(l-h)d}\right]}{\left[1 + \Gamma_1\Gamma_2 e^{-2jk_{zc}(l-h)d}\right]} \\
V_4 &= \frac{V_2 T_1 e^{-jk_{za}hd}}{1 + \Gamma_1\Gamma_2 e^{-2jk_{zc}(l-h)d}} \\
V_5 &= \frac{V_2 \Gamma_2 T_1 e^{-jk_{za}hd}}{\Gamma_1\Gamma_2 + e^{2jk_{zc}(l-h)d}} \\
V_6 &= \frac{V_2 T_1 T_2 e^{-jk_{za}hd}}{e^{jk_{zc}(l-h)d} + \Gamma_1\Gamma_2 e^{-jk_{zc}(l-h)d}}.
\end{aligned} \tag{9}
$$

The expressions Γ_1 and Γ_2 are essentially the reflection coefficients initially seen by an incident voltage wave at the first and second interfaces, respectively, while T_1 and T_2 are the corresponding transmission coefficients. They are given by the following expressions:

$$
\begin{aligned}
\Gamma_1 &= \frac{Z_{zc} - Z_{za}}{Z_{zc} + Z_{za}} \\
\Gamma_2 &= \frac{Z_{zd} - Z_{zc}}{Z_{zd} + Z_{zc}} \\
T_1 &= \frac{2Z_{zc}}{Z_{za} + Z_{zc}} \\
T_2 &= \frac{2Z_{zd}}{Z_{zc} + Z_{zd}}.
\end{aligned} \tag{10}
$$

By setting $k_{xa}d = k_{xc}d = k_{xd}d = \xi$, the wavenumbers k_{za} and k_{zd} are found using dispersion relation 1, and k_{zc} is found using dispersion relation 4, shown in (11) and (12) at the bottom of this page. For propagating waves, the signs ($+$ or $-$) of these wavenumbers are chosen such that the z-directed Bloch impedances (Z_{za}, Z_{zc}, Z_{zd}) in (9) and (10) are positive quantities.

The z-directed terminal currents $I(md, nd)$ generated by the current array excitation can also be evaluated in the four regions by dividing the voltage expressions of (8) by the z-directed Bloch impedances of the corresponding media

$$
\begin{aligned}
I(md, nd) &= \frac{V_1}{Z_{za}} e^{jk_{za}nd} e^{-jm\xi}, \qquad z \leq 0 \text{ (region A)} \\
I(md, nd) &= \left[\frac{V_2}{Z_{za}} e^{-jk_{za}nd} - \frac{V_3}{Z_{za}} e^{jk_{za}nd}\right] e^{-jm\xi}, \\
&\qquad 0 \leq z \leq hd \text{ (region B)} \\
I(md, nd) &= \left[\frac{V_4}{Z_{zc}} e^{-jk_{zc}(n-h)d} - \frac{V_5}{Z_{zc}} e^{jk_{zc}(n-h)d}\right] e^{-jm\xi}, \\
&\qquad hd \leq z \leq ld \text{ (region C)}
\end{aligned}
$$

$$
\begin{aligned}
I(md, nd) &= \frac{V_6}{Z_{zd}} e^{-jk_{zd}(n-l)d} e^{-jm\xi}, \\
&\qquad z \geq ld \text{ (region D).} \tag{13}
\end{aligned}
$$

In the particular case of the "perfect lens," $Z_{za} = Z_{zc} = Z_{zd}$ and $k_{za} = k_{zc} = -k_{zd}$ for propagating waves. Under these conditions, there are no reflections at the two interfaces, therefore, $\Gamma_1 = \Gamma_2 = 0$ and $T_1 = T_2 = 1$. This implies that the reflected waves $V_3 = V_5 = 0$. For evanescent waves, $Z_{za} = Z_{zc} = Z_{zd}$ and $k_{za} = k_{zc} = k_{zd}$. As a result, $\Gamma_1 = \Gamma_2 = 0, T_1, T_2$ become infinite and $V_3 = V_4 = 0$. For the "perfect lens," (8) simplifies to

$$
\begin{aligned}
V(md, nd) &= \frac{I_o Z_{za}}{2} e^{jk_{za}nd} e^{-jm\xi}, \qquad z \leq 0 \text{ (region A)} \\
V(md, nd) &= \frac{I_o Z_{za}}{2} e^{-jk_{za}nd} e^{-jm\xi}, \\
&\qquad 0 \leq z \leq hd \text{ (region B)} \\
V(md, nd) &= \frac{I_o Z_{za}}{2} e^{jk_{za}(n-2h)d} e^{-jm\xi}, \\
&\qquad hd \leq z \leq ld \text{ (region C)} \\
V(md, nd) &= \frac{I_o Z_{za}}{2} e^{-jk_{za}(n-2(l-h))d} e^{-jm\xi}, \\
&\qquad z \geq ld \text{ (region D).} \tag{14}
\end{aligned}
$$

The voltage expression for region C (14) shows that the source–plane voltage (voltage along $z = 0$) is recovered at $z = 2hd$ ($n = 2h$). This corresponds to the location of the internal focal plane of the dual-TL lens. Equivalently, the voltage expression for region D (14) indicates that the source–plane voltage is again recovered at $z = 2(l - h)d$ ($n = 2l - 2h$), corresponding to the location of the external focal plane.

A. Phase Compensation of Propagating Waves

Equation (14) has assumed that there is perfect impedance matching and that an exact relative refractive index of -1 exists between the TL mesh and dual-TL structure. In Fig. 6, the phases of the terminal voltages in all four regions (A–D) are shown for the flat-lens system of Fig. 5 made of the TL mesh and dual-TL structure defined in Table I. In these calculations, the amplitude of the current sources is set to 34.5 mA so that the voltage amplitude $|V_2| = 1$ V at $z = 0$. The progressive phase shift of the current sources is set to $\xi = 0.17455$ rad. According to (7), this progressive phase shift ξ excites a plane wave in Region B incident at an angle of $\phi_o = \pi/6$ rad. As in Fig. 5, the values $h = 2$ and $l = 6$ are used in the computation. The voltage phase progression in Fig. 6 clearly shows the negative refraction of a propagating plane wave incident at $\pi/6$ rad. As anticipated, the phase of the incident plane wave ($z = 0$) is restored along the internal ($z = 2hd = 4d$) and external focal plane ($z = 2(l - h)d = 8d$). Therefore, the lens acts as a phase

$$
\left.\begin{aligned} k_{za}d \\ k_{zd}d \end{aligned}\right\} = 2\sin^{-1}\left(\sqrt{2\sin^2\left(\frac{\beta d}{2}\right) - \sin^2\left(\frac{\xi}{2}\right)}\right) \tag{11}
$$

$$
k_{zc}d = 2\sin^{-1}\left(\sqrt{\frac{1}{2}\left[2\sin\left(\frac{\beta d}{2}\right) - \frac{1}{Z_o\omega C}\cos\left(\frac{\beta d}{2}\right)\right]\left[2\sin\left(\frac{\beta d}{2}\right) - \frac{Z_o}{2\omega L}\cos\left(\frac{\beta d}{2}\right)\right] - \sin^2\left(\frac{\xi}{2}\right)}\right) \tag{12}
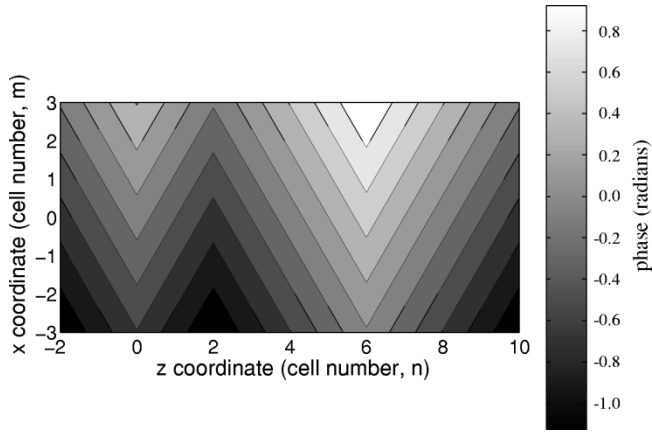$$

Fig. 6.   Voltage phases in regions A–D for a propagating plane-wave excitation.

compensator for propagating plane waves, as would a conventional lens.

B. Growth and Restoration of Evanescent Waves

Next, a progressive phase shift ξ exceeding $k_a d$ is considered. This implies that the transverse wavenumber $k_{xa} = \xi/d$ exceeds the intrinsic wavenumber k_a in regions A and B. Therefore, the array of current sources excites an evanescent wave. In other words, the z-directed wavenumber takes the form $k_{za} = -j\alpha$. The voltage expression for region C in (14), therefore, becomes

$$V(md, nd) = \frac{I_o Z_{za}}{2} e^{\alpha(n-2h)d} e^{-jm\xi},$$
$$hd \leq z \leq ld \text{ (region C)}. \qquad (15)$$

Equation (15) indicates a growing evanescent wave within the dual-TL lens, as was predicted by Pendry [2] for an NRI lens. In the same manner, it can also be shown that the voltages in regions A, B, and D are decaying waves. Fig. 7 plots the magnitude of the terminal voltages for a current array excitation with progressive phase shift $\xi = 0.4161$ rad. The TL mesh and dual-TL structure defined in Table I are used once again in this calculation. According to (1), this ξ corresponds to $\alpha d = 0.2231$ Np. The current amplitude is set to $I_o = 25.3$ mA in order to yield a voltage amplitude of $|V_2| = 1$ V at $z = 0$. As anticipated, the voltage plot indicates a growing evanescent wave within the dual-TL lens (region C) and decaying evanescent waves in the TL mesh regions (A, B, and D). This is in direct agreement with the previously reported microwave circuit simulations results of [14]. Along the internal ($z = 2hd = 4d$) and external ($z = 2(l - h)d = 8d$) focal planes, the amplitude of the source evanescent wave ($z = 0$) is restored. Therefore, unlike a conventional curved lens, the dual-TL lens restores the amplitude of evanescent waves, which is a unique characteristic of Pendry's "perfect lens."

IV. SUB-DIFFRACTION IMAGING OF AN ELEMENTARY CURRENT SOURCE: GREEN'S FUNCTIONS DERIVATION

In the previous section, voltage and current solutions were derived for a current array excitation. Here, a transformation known as "analytical array scanning" [17], [18] is applied to
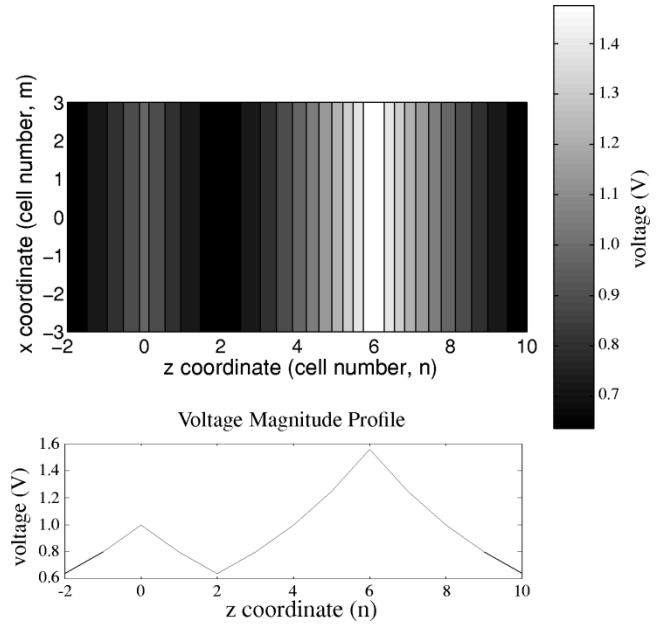

Voltage Magnitude Profile

Fig. 7.   Voltage magnitudes in regions A–D for an evanescent wave excitation.

these solutions to find the Green's functions or voltage and current solutions due to a single y-directed current source. The terminal voltages in all four regions (A–D) of the dual-TL lens caused by a single current source excitation at the origin can be found by integrating the voltage solutions of (8) between $-\pi \leq \xi \leq \pi$ as follows:

$$V'(md, nd)$$
$$= \frac{1}{2\pi} \int_{-\pi}^{\pi} V_1 e^{jk_{za}nd} e^{-jm\xi} \, d\xi, \qquad z \leq 0$$
$$V'(md, nd)$$
$$= \frac{1}{2\pi} \int_{-\pi}^{\pi} \left[V_2 e^{-jk_{za}nd} + V_3 e^{jk_{za}nd} \right] e^{-jm\xi} \, d\xi,$$
$$0 \leq z \leq hd$$
$$V'(md, nd)$$
$$= \frac{1}{2\pi} \int_{-\pi}^{\pi} \left[V_4 e^{-jk_{zc}(n-h)d} + V_5 e^{jk_{zc}(n-h)d} \right] e^{-jm\xi} \, d\xi,$$
$$hd \leq z \leq ld$$
$$V'(md, nd)$$
$$= \frac{1}{2\pi} \int_{-\pi}^{\pi} V_6 e^{-jk_{zd}(n-l)d} e^{-jm\xi} \, d\xi, \qquad z \geq ld. \qquad (16)$$

The integration in (16) represents a superposition of phased current-array solutions spanning the entire phase space $-\pi \leq \xi \leq \pi$. This integration cancels out all the current sources in the infinite array along $z = 0$, except for the one located at $x = 0$, which has a zero phase angle. The cancellation of current sources occurs due to the simple fact that

$$\frac{1}{2\pi} \int_{-\pi}^{\pi} e^{jq\psi} \, d\psi = \begin{cases} 1, & q = 0 \\ 0, & q \neq 0. \end{cases} \qquad (17)$$

Given the conditions of perfect focusing, the source plane voltages at $z = 0$ are imaged exactly to the internal ($z = 2hd$)
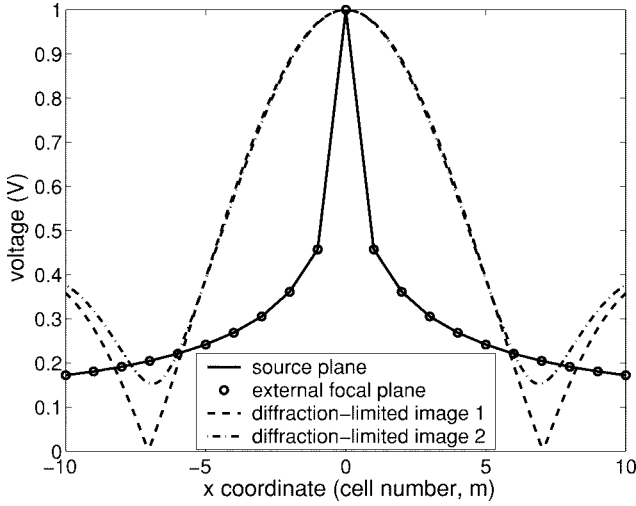
Fig. 8. Voltage magnitudes at the source plane ($n = 0$) and external focal plane ($n = 8$).

Fig. 9. Voltage magnitude distribution for the three-region TL lens.

and external focal planes ($z = 2(l - h)d$). Using (16), the voltages at the source plane and both the internal and external focal planes are

$$V' = \frac{I_o}{4\pi} \int_{-\pi}^{\pi} Z_{za}(\xi) e^{-jm\xi} \, d\xi. \tag{18}$$

In (18), it is important to remember that the Bloch impedance Z_{za} [given by (3)] is a function of ξ due to the fact that k_{za} and ξ are related through dispersion (11). The terminal voltage magnitudes at the source and external focal plane are shown in Fig. 8 for the flat lens system depicted in Fig. 5. These voltages are computed using (16) for the TL mesh and dual-TL structure defined in Table I. In the computation, the magnitude of the current source was set to 14.6 mA in order to yield a voltage magnitude of 1 V at the source. As shown in Fig. 5, the terminal voltages along the external focal plane are identical to those at the source plane. The standard diffraction-limited image (diffraction limited image 1) is also shown in Fig. 8 for comparative purposes. It is obtained by inverse Fourier transforming the propagating spectrum of the source in a continuous medium [23] with the identical effective material parameters. Due to the close proximity of the source and image, a second diffraction-limited image (diffraction-limited image 2) has also been shown in Fig. 8, which takes into account the attenuated evanescent waves that reach the external focal plane. For this latter diffraction-limited image, the propagating Fourier components emanating from the source are focused, whereas the evanescent components are not neglected, but rather assumed to exponentially decay from source to image with attenuation factors corresponding to a relative refractive index of $n = +1$. The image obtained with the dual-TL lens clearly shows finer resolution than both diffraction-limited images. Therefore, this practical microwave lens using TLs acts as a "superlens" allowing imaging beyond the diffraction limit.

Equation (18) may also be used to determine the input impedance to the network. It can be found by setting $m = 0$ and dividing the result by I_o. In general, the terminal impedance at
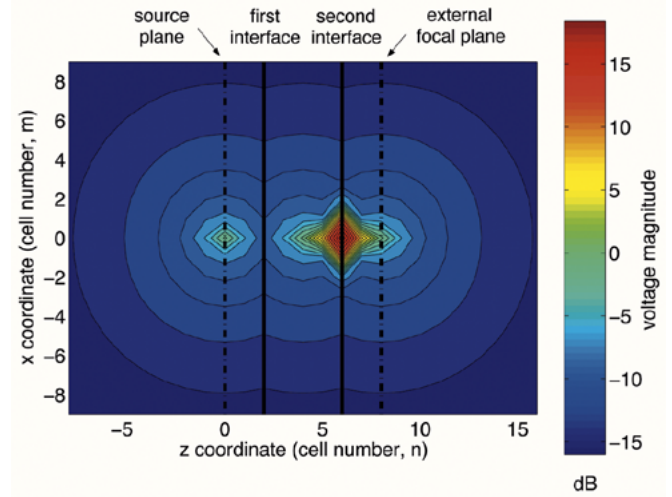
an arbitrary point $(x, z) = (md, nd)$ can be found by evaluating $V'(md, nd)$ and $I'(md, nd)$ and computing their ratio. The current $I'(md, nd)$ is the terminal current at $(x, z) = (md, nd)$ due to the current source excitation at the origin. It can be found by integrating (13) between $-\pi \leq \xi \leq \pi$.

To gain a better understanding of sub-diffraction imaging, it is useful to observe the entire voltage solution. Fig. 9 depicts the voltage magnitudes (in decibels) at the terminals of all the unit cells in the entire structure, computed by solving the integrals in (16). Most notably, high-voltage amplitudes are apparent near the second interface ($n = 6$) due to the growing evanescent waves in the dual-TL structure. In addition, the voltage amplitudes far from the central row ($m = 0$) form three distinct cylindrical waves with phase centers that clearly identify the source $[n, m] = [0, 0]$, the internal focus $[n, m] = [4, 0]$ in the dual-TL structure (NRI medium), and the external focus $[n, m] = [8, 0]$ in the TL mesh (PRI medium), as designated in Fig. 2. The voltage magnitude distribution of Fig. 9, which was obtained here analytically, is corroborated by the microwave-circuit simulations presented in [24]. The focusing results utilizing the three-region dual-TL lens presented in this paper are dramatically different from those previously observed in the two-region dual-TL lenses of [11] and [21]. Unlike in the previous two-region lenses, the focusing reported here is dominated by the growth of evanescent waves and clearly shows sub-diffraction resolution.

V. EFFECT OF PERIODICITY ON IMAGE RESOLUTION AND THE MAXIMUM AMPLITUDE OF THE EVANESCENT WAVES

The voltage solutions of (16) indicate that the periodicity of the PRI and NRI media impose a resolution limit. The maximum resolution (Δ) at the focal plane of a lens is [2]

$$\Delta \approx \frac{2\pi}{k_{\max}} \tag{19}$$

where $k_{\max}$ is the maximum transverse (x-directed) propagation constant. According to the integration limits of (19), the

maximum x-directed wavenumber is $k_{xa} = \xi/d = \pi/d$. This yields a maximum resolution limit of

$$\Delta \approx \frac{2\pi}{k_{\max}} \approx 2d. \tag{20}$$

Therefore, a resolution of $\lambda/10$ would require a periodicity of at least $d = \lambda/20$. This is in agreement with the resolution enhancement calculations derived in [25]. For the lens system shown in Fig. 5, $k_{\max}$ is limited right at the source point. This occurs because, in addition to the lens being periodic, the PRI medium (TL mesh), in which the current source is embedded, is also periodic. This explains why there is no apparent loss in resolution at the focal planes in (18). On the other hand, if the source were in a continuous medium, the resolution would only be limited by the periodicity of the NRI lens. In this case, "perfect" imaging could not be achieved, but sub-diffraction imaging would still be possible. Other physical constraints such as losses and mismatches due to manufacturing tolerances would also have to be accounted for in any practical lens system [11], [20], [25].

It is important to realize that $k_{\max}$ in turn places a limit on α, the "amplification" factor of the evanescent waves [see (15)]. This limitation on α prevents the voltages and currents from growing to unphysically large values at the second interface of a practical lens having finite thickness $(ld - hd)$, an objection to the "perfect lens" raised in [26]. In fact, the periodicity provides a natural mechanism by which the amplitudes of the evanescent waves are limited. The finer the periodicity, the larger the maximum amplitude of the growing evanescent waves and the higher the resolution.

VI. CONCLUSION

The negative refraction of propagating waves and the growth of evanescent waves were shown analytically for an NRI lens implemented using a loaded-TL periodic structure: the dual-TL structure. These homogeneous and inhomogeneous plane-wave-type solutions were then combined using the "array scanning method" to analytically demonstrate sub-diffraction focusing by the dual-TL lens. This entailed determining the 2-D periodic Green's functions of the system corresponding to the voltages and currents (at the unit cell terminals) generated by a single vertical elementary current source. In addition to showing that the voltage distribution at the external focal plane is identical to that at the source plane, 2-D plots of the entire voltage solution have been included, which aid in understanding the nature of sub-diffraction imaging. The analysis also revealed that a resolution limit is imposed by the periodicity of a real NRI lens. Finally, it was shown that the periodicity of the lens bounds the amplitude of the growing evanescent waves in a realizable NRI lens of finite thickness. As a result, the evanescent waves do not grow to unphysically large values.

REFERENCES

[1] V. G. Veselago, "The electrodynamics of substances with simultaneously negative values of ϵ and μ," *Sov. Phys.—Usp.*, vol. 10, pp. 509–514, Jan.–Feb. 1968.

[2] J. B. Pendry, "Negative refraction makes a perfect lens," *Phys. Rev. Lett.*, vol. 85, pp. 3966–3969, Oct. 2000.

[3] R. A. Shelby, D. R. Smith, and S. Schultz, "Experimental verification of a negative index of refraction," *Science*, vol. 292, pp. 77–79, Apr. 2001.

[4] A. K. Iyer and G. V. Eleftheriades, "Negative refractive index metamaterials supporting 2-D wave propagation," in *IEEE MTT-S Int. Microwave Symp. Dig.*, vol. 2, Seattle, WA, June 2–7, 2002, pp. 1067–1070.

[5] G. V. Eleftheriades, A. K. Iyer, and P. C. Kremer, "Planar negative refractive index media using periodically L–C loaded transmission lines," *IEEE Trans. Microwave Theory Tech.*, vol. 50, pp. 2702–2712, Dec. 2002.

[6] A. Grbic and G. V. Eleftheriades, "Dispersion analysis of a microstrip-based negative refractive index periodic structure," *Microwave Wireless Comp. Lett.*, vol. 13, pp. 155–157, Apr. 2003.

[7] S. Ramo, J. R. Whinnery, and T. Van Duzer, *Fields and Waves in Communication Electronics*, 3rd ed. New York: Wiley, 1994.

[8] A. Grbic and G. V. Eleftheriades, "A backward-wave antenna based on negative refractive index L–C networks," in *IEEE Int. AP-S Symp.*, vol. 4, San Antonio, TX, June 16–21, 2002, pp. 340–343.

[9] C. Caloz, H. Okabe, H. Iwai, and T. Itoh, "Transmission line approach of left-handed materials," in *USNC/URSI Nat. Radio Science Meeting*, San Antonio, TX, June 16–21, 2002, p. 39.

[10] A. A. Oliner, "A periodic-structure negative-refractive-index medium without resonant elements," in *USNC/URSI Nat. Radio Science Meeting*, San Antonio, TX, June 16–21, 2002, p. 41.

[11] A. K. Iyer, A. Grbic, and G. V. Eleftheriades, "Sub-wavelength focusing in transmission line loaded negative refractive index metamaterials," in *IEEE MTT-S Int. Microwave Symp. Dig.*, vol. 1, Philadelphia, PA, June 8–13, 2003, pp. 199–202.

[12] A. Grbic and G. V. Eleftheriades, "Experimental verification of backward-wave radiation from a negative refractive index metamaterial," *J. Appl. Phys.*, vol. 92, pp. 5930–5935, Nov. 2002.

[13] ——, "Periodic analysis of a 2-D negative refractive index transmission line structure," *IEEE Trans. Antennas Propagat.*, vol. 51, pp. 2604–2611, Oct. 2003.

[14] ——, "Growing evanescent waves in negative-refractive-index transmission-line media," *Appl. Phys. Lett.*, vol. 82, no. 12, pp. 1815–1817, Mar. 2003.

[15] K. G. Balmain, A. E. Luttgen, and P. C. Kremer, "Resonance cone formation, reflection, refraction and focusing in a planar, anisotropic metamaterial," *IEEE Antennas Wireless Propagat. Lett.*, vol. 1, pp. 146–149, July 2002.

[16] D. R. Smith and D. Schurig, "Electromagnetic wave propagation in media with indefinite permittivity and permeability tensors," *Phys. Rev. Lett.*, vol. 90, p. 077 405, Feb. 2003.

[17] B. A. Munk and G. A. Burrell, "Plane-wave expansion for arrays of arbitrarily oriented piecewise linear elements and its applications in determining the impedance of a single linear antenna in a lossy half-space," *IEEE Trans. Antennas Propagat.*, vol. AP-27, pp. 331–343, May 1979.

[18] H. Y. D. Yang, "Theory of antenna radiation from photonic band-gap materials," *Electromagnetics*, vol. 19, pp. 255–276, May–June 1999.

[19] R. W. Ziolkowski and E. Heyman, "Wave propagation in media having negative permittivity and permeability," *Phys. Rev. E, Stat. Phys. Plasmas Fluids Relat. Interdiscip. Top.*, vol. 64, p. 056 625, Oct. 2001.

[20] N. Fang and X. Zhang, "Imaging properties of a metamaterial superlens," *Appl. Phys. Lett.*, vol. 82, pp. 161–163, Jan. 2003.

[21] J. B. Pendry and S. A. Ramakrishna, "Near-field lenses in two dimensions," *J. Phys. Condens. Matter*, vol. 14, pp. 8463–8479, 2002.

[22] A. K. Iyer, P. C. Kremer, and G. V. Eleftheriades, "Experimental and theoretical verification of focusing in a large, periodically loaded transmission line negative refractive index metamaterial," *Opt. Express*, vol. 11, pp. 696–708, Apr. 2003.

[23] S. A. Cummer, "Simulated causal subwavelength focusing by a negative refractive index slab," *Appl. Phys. Lett.*, vol. 82, pp. 1503–1505, Mar. 2003.

[24] A. Grbic and G. V. Eleftheriades, "Subwavelength focusing using a negative-refractive-index transmission-line lens," *IEEE Antennas Wireless Propagat. Lett.*, vol. 2, pp. 186–189, 2003.

[25] D. R. Smith, D. Schurig, R. Rosenbluth, S. Schultz, S. A. Ramakrishna, and J. B. Pendry, "Limitations on subdiffraction imaging with a negative refractive index slab," *Appl. Phys. Lett.*, vol. 82, pp. 1506–1508, Mar. 2003.

[26] G. W. 't Hooft, "Comment on negative refraction makes a perfect lens," *Phys. Rev. Lett.*, vol. 87, p. 249701, Dec. 2001.

Anthony Grbic (S'00) received the B.A.Sc. and M.A.Sc. degrees in electrical engineering from the University of Toronto, Toronto, ON, Canada, in 1998 and 2001, respectively, and is currently working toward the Ph.D. degree at the University of Toronto.

His research interests include planar millimeter-wave antennas, microwave circuits, NRI metamaterials and periodic structures.

Mr. Grbic was the recipient of the 2000 Best Student Paper Award presented at the Antenna Technology and Applied Electromagnetics Symposium.

George V. Eleftheriades (S'86–M'88–SM'02) received the Diploma (with distinction) in electrical engineering from the National Technical University of Athens, Athens, Greece in 1988, and the Ph.D. and M.S.E.E. degrees in electrical engineering from The University of Michigan at Ann Arbor, in 1993 and 1989, respectively.

From 1994 to 1997, he was with the Swiss Federal Institute of Technology, Lausanne, Switzerland, where he was engaged in the design of millimeter and sub-millimeter-wave receivers and in the creation of fast computer-aided design (CAD) tools for planar packaged microwave circuits. He is currently an Associate Professor with the Department of Electrical and Computer Engineering, University of Toronto, Toronto, ON, Canada. He has authored or coauthored over 80 papers in refereed journals and conference proceedings. His current research interests include NRI metamaterials, integrated circuit (IC) antennas and components for broad-band wireless communications, novel beam-steering techniques, low-loss silicon micromachined components, millimeter-wave radiometric receivers, and electromagnetic design for high-speed digital circuits.

Dr. Eleftheriades was a corecipient of the 1990 Best Paper Award presented at the 6th International Symposium on Antennas (JINA) and the Ontario Premier's 2001 Research Excellence Award. His graduate students were the recipients of Student Paper Awards presented at the 2000 Antenna Technology and Applied Electromagnetics Symposium, the 2002 IEEE Microwave Theory and Techniques Society (IEEE MTT-S) International Microwave Symposium (IMS), and the 2002 IEEE International Symposium on Antennas and Propagation.